frontiers | Frontiers in Earth Science

TYPE Original Research
PUBLISHED 06 September 2022
DOI 10.3389/feart.2022.963086

OPEN ACCESS

EDITED BY
Pascal Boivin,
University of Applied Sciences Western Switzerland, Switzerland

REVIEWED BY
Bing Bai,
Beijing Jiaotong University, China
Sujatha Evangelin Ramani,
SASTRA University, India
Jia-wen Zhou,
Sichuan University, China

*CORRESPONDENCE
Yanbo Zhu,
zhuyanbo@chd.edu.cn
Hengxing Lan,
Lanhx@igsnrr.ac.cn

SPECIALTY SECTION
This article was submitted to Geohazards and Georisks, a section of the journal Frontiers in Earth Science

RECEIVED 07 June 2022
ACCEPTED 15 August 2022
PUBLISHED 06 September 2022

CITATION
Zhu Y, Zheng H, Lan H, Liu Y, Li L, Fu B and Du C (2022), Effect of initial water content and dry density on the self-healing of desiccation cracks in compacted hipparion red clay. *Front. Earth Sci.* 10:963086. doi: 10.3389/feart.2022.963086

Effect of initial water content and dry density on the self-healing of desiccation cracks in compacted hipparion red clay

Yanbo Zhu[1]*, Huitao Zheng[1], Hengxing Lan[1,2]*, Yaowen Liu[1], Langping Li[2], Boyu Fu[1] and Changcheng Du[1]

[1]College of Geological Engineering and Geomatics, Chang'an University, Xi'an, China, [2]State Key Laboratory of Resources and Environmental Information System, Institute of Geographic Sciences and Natural Resources Research, CAS, Beijing, China

The self-healing of desiccation cracks in compacted clayey soils is important for mechanism revelation of cracking behavior in compacted soils. Although the crack self-healing behavior has been found, the influence of soil physical indices on it is still unclear, especially initial water content and dry density of specimen. This study aims to identify and evaluate the effect of initial water content and dry density on self-healing of desiccation cracks. Firstly, a series of desiccation tests were conducted on compacted Hipparion red clay specimens under different initial conditions. Secondly, the two-dimensional morphology of desiccation cracks and strain field changes on specimen surface were examined using the pore and crack analysis system and digital image correlation techniques. The result shows that the desiccation cracks on specimen surface exhibits self-healing behavior during drying. Based on the observed crack self-healing behavior, the desiccation cracking of compacted Hipparion red clay undergoes four stages including initiation, development, self-healing, and stabilization. During the self-healing stage, the critical water content for occurrence of crack self-healing and the crack self-healing amount referring to the crack ratio reduction from peak value to the stable value, are dry density dependent and water content dependent variables. In particular, the higher the initial water content and the lower the dry density of compacted specimen are, the larger the crack self-healing amount is. This crack self-healing difference in specimen with different initial conditions is caused by the vertical anisotropic shrinkage of substrate soil below non-propagating cracks due to its pore structure difference. This study provides a new perspective on the mechanism of desiccation crack in clayey soils affected by initial conditions.

KEYWORDS

Hipparion red clay, desiccation crack, crack self-healing, critical water content, self-healing amount

1 Introduction

Desiccation cracking of clay soils is a common natural phenomenon, and extensive studies on desiccation cracking have been conducted in various fields (Miller et al., 1998; Yesiller et al., 2000; Tang et al., 2007, Tang et al., 2011b, Tang et al., 2021; Zhang et al., 2019). Based on the theory of crack evolution (Morris et al., 1992; Vo et al., 2017), a large number of experimental studies were conducted on the initiation and propagation of desiccation cracks in soils (Albrecht and Benson., 2001; Tang et al., 2007; Kaufhold et al., 2015; Tollenaar et al., 2017; Levatti et al., 2019). Saturated slurry specimens were often used in these experimental studies owing to their simple specimen preparation, high reproducibility, and low interference (Tang et al., 2008; Goehring et al., 2010; DeCarlo and Shokri., 2014). Many prior works refer to initially saturated slurry samples, whereas most of the geotechnical constructions prone to cracking involve compacted soils (Demagistri et al., 2018). Therefore, the cracking behavior of soils in an actual geological environment can be more accurately reflected by using compacted specimens (Krisdani et al., 2008; Lakshmikantha et al., 2012).

Notably, some studies show that the cracks pattern of compacted clay specimens differs from the slurry specimens (Nahlawi and Kodikara., 2006; Costa et al., 2013a; Wei L. et al., 2020). For example, majority of the desiccation cracks in dried slurries extend from the top to bottom surface (Tang et al., 2010; Costa et al., 2013b; Tang et al., 2018). However, from the works of Day, (1997, Day, 1998), Miller et al. (1998), Rao et al. (2000), Yesiller et al. (2000) and Auvray et al. (2014), it is evident that not all the desiccation cracks run through the entire compacted specimens due to the high tensile strength of soli specimen. Thus, some complexity cracking behaviors have been observed (Tang et al., 2011b; Tabassum and Bheemasetti, 2020), such as the self-healing behavior of cracks within compacted clay specimen (Chertkov et al., 2004; Boivin, 2007; Du et al., 2019; Julina and Thyagaraj, 2019, 2020, 2021; Li et al., 2020; Tan et al., 2020). In particular, the desiccation cracks in compacted specimen tended to close at the end of shrinkage stage during drying (Chertkov et al., 2004; Boivin, 2007). Du et al. (2019) and Tan et al. (2020) used the photography technology to capture the self-healing behaviors of desiccation cracks in compacted cohesive soils and bentonite soils during drying, and they divided the evolution of soil cracking upon drying into four stages including crack growth, maintenance, closure and stabilization stage. Julina and Thyagaraj (2019, 2021) introduced the XCT imaging and vernier caliper height method for tracing the shrinkage behavior of compacted expansive soil specimen, and they also found the phenomenon that the cracks area and cracks volume first increased and then decreased during drying.

The self-healing of desiccation crack within compacted samples mentioned above is different from that in some previous studies, which mainly reported the self-healing of cracks within compacted samples subjected to wet-dry cycles (Day, 1994; Al-Homoud et al., 1995; Basma et al., 1996; Rao et al., 2000; Tripathy et al., 2002; Nowamooz and Masrouri., 2008,2010a; Tripathy and Subba Rao, 2009; Thyagaraj and Zodinsanga, 2014), or within treated samples containing different additives (Guo et al., 2018; Vail et al., 2019; Tabassum and Bheemasetti, 2020). The occurrence of crack self-healing of specimen during a single drying indicates that the mechanism of cracking in compacted soil is a complex process. Du et al. (2019) reported the cracking behavior of compacted soil not only depends on the tensile stress and tensile strength of cracking regions, but also depends on the overall shrinkage of the lower parts under cracking regions closely. However, there seems to be no fundamental explanation available for the phenomenon of crack closure that was observed in present experiments (Tan et al., 2020). Therefore, the self-healing of desiccation cracks is important for mechanism revelation of cracking in compacted soils and needs examination studies.

There are many factors that affect the initiation and propagation of cracks in compacted specimens such as specimen dimensions, boundary conditions, temperature effect (Bai et al., 2021, 2022), and soil properties (Cheng et al., 2020; Wei X. et al., 2020). The crack self-healing is also affected by some soil physical indices such as water content. The area and width of non-propagating cracks in compacted samples increased until a specific water content during drying and decreased with continuous drying later (Julina and Thyagaraj, 2018; Julina and Thyagaraj, 2019; Julina and Thyagaraj, 2021). This specific water content is a critical water content for self-healing of cracks within compacted specimens, and it was found as a non-constant value (Du et al., 2019). Although the water content influencing crack self-healing has been found, the quantitative influence of soil physical indices is still unclear, especially initial water content and initial dry density of specimen.

This study aims to identify and evaluate the effect of water content and dry density on self-healing of desiccation cracks in compacted Hipparion red clay. Firstly, an experimental investigation of desiccation cracking of compacted Hipparion red clay was conducted using a purpose-made drying device, and the process of water evaporation in soil was analyzed. Secondly, the evolution of desiccation cracks and strain field changes of specimen were quantitatively analyzed using the pore and crack analysis system and the digital image correlation technique, and the evolution stages of cracking were discussed. Finally, the critical water content for occurrence of crack self-healing and self-healing amount referring to the reduction value of crack ratio from peak value to the stable value were defined for evaluating the effect of initial water content and dry density on crack self-healing. This study provides a new perspective on the mechanism of desiccation crack in clayey soils affected by initial conditions.

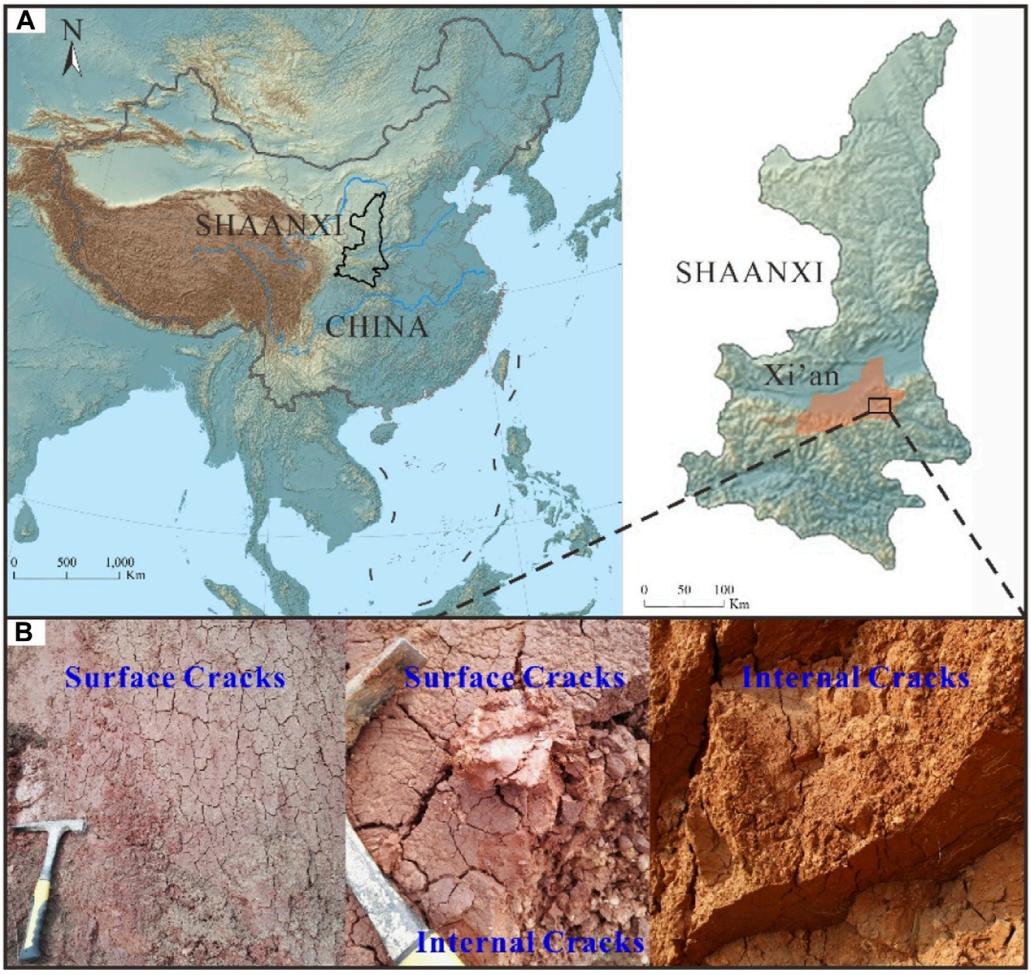

FIGURE 1
Sampling site of the Hipparion red clay. **(A)** Location of the study site, and **(B)** Desiccation cracks in Hipparion red clay.

2 Materials and methods

2.1 Soil materials

The soil material for desiccation cracking test is Hipparion red clay collected from the Bailu loess tableland in Xi'an (Figures 1A,B). The Hipparion red clay is characterized by water swelling and drying shrinkage due to its clayey composition (Li et al., 2013). The Hipparion red clay undergo large volumetric changes during wet-dry cycles owing to the seasonal moisture fluctuations, and during drying the shrinkage is accompanied with the desiccation cracks (Figure 1C). The basic physical properties of the Hipparion red clay are as follows: the specific gravity is 2.73, the liquid limit is 44.90%, the plastic limit is 25.10%, the plasticity index is 19.80, the dry density is 1.93 g/cm^3, and the free swell index of the soil is 40.5%. The natural moisture content and optimal moisture content of the Hipparion red clay are 13% and 15.3% respectively. The particle size distribution of the Hipparion red clay is shown in Figure 2, indicating that the soil material consists of clay (particle diameter less than 0.005 mm), silt (particle diameter between 0.005 mm and 0.075 mm), and sand (particle diameter more than 0.075 mm), with contents of 51.29%, 48.67%, and 0.04% respectively. The X-ray diffraction test shows that the clay mineral content of Hipparion red clay is 40.7%, and the montmorillonite-illite mixed layer mineral content is 28.9%. Therefore, the Hipparion red clay has the swelling and shrinkage behaviors during wet-dry cycles.

2.2 Specimen preparation

After collected from the field, the soil material was air-dried, crushed and sieved through a 1-mm mesh sieve in the laboratory.

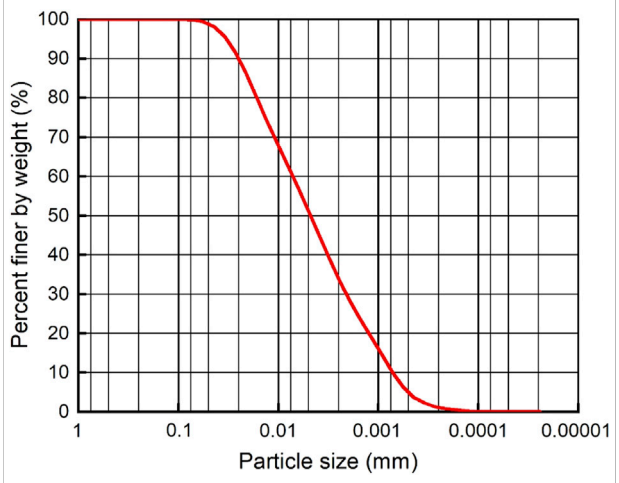

FIGURE 2
Particle size distribution of the Hipparion red clay.

The compacted specimens were prepared for the laboratory testing (Figure 3). The required quantity of distilled water was used to uniformly pre-wet the Hipparion red clay. For moisture equilibration, the pre-wetted soil was stored in sealed plastic covers for at least 48 h. Then the identical compacted specimens were prepared by compacting the pre-wetted soil in rigid rings (diameter: 61.8 mm, height: 20 mm). To better reveal the effect of initial conditions on the cracking behavior of compacted Hipparion red clay specimens, the desiccation test differing initial water contents, dry densities of compacted specimens were designed as shown in Table 1.

2.3 Test procedure

The research of desiccation cracks of compacted Hipparion red clay composed of desiccation testing of specimens, quantitative analysis of desiccation cracks, strain filed analysis on specimen surface (Figure 3). Desiccation test of compacted

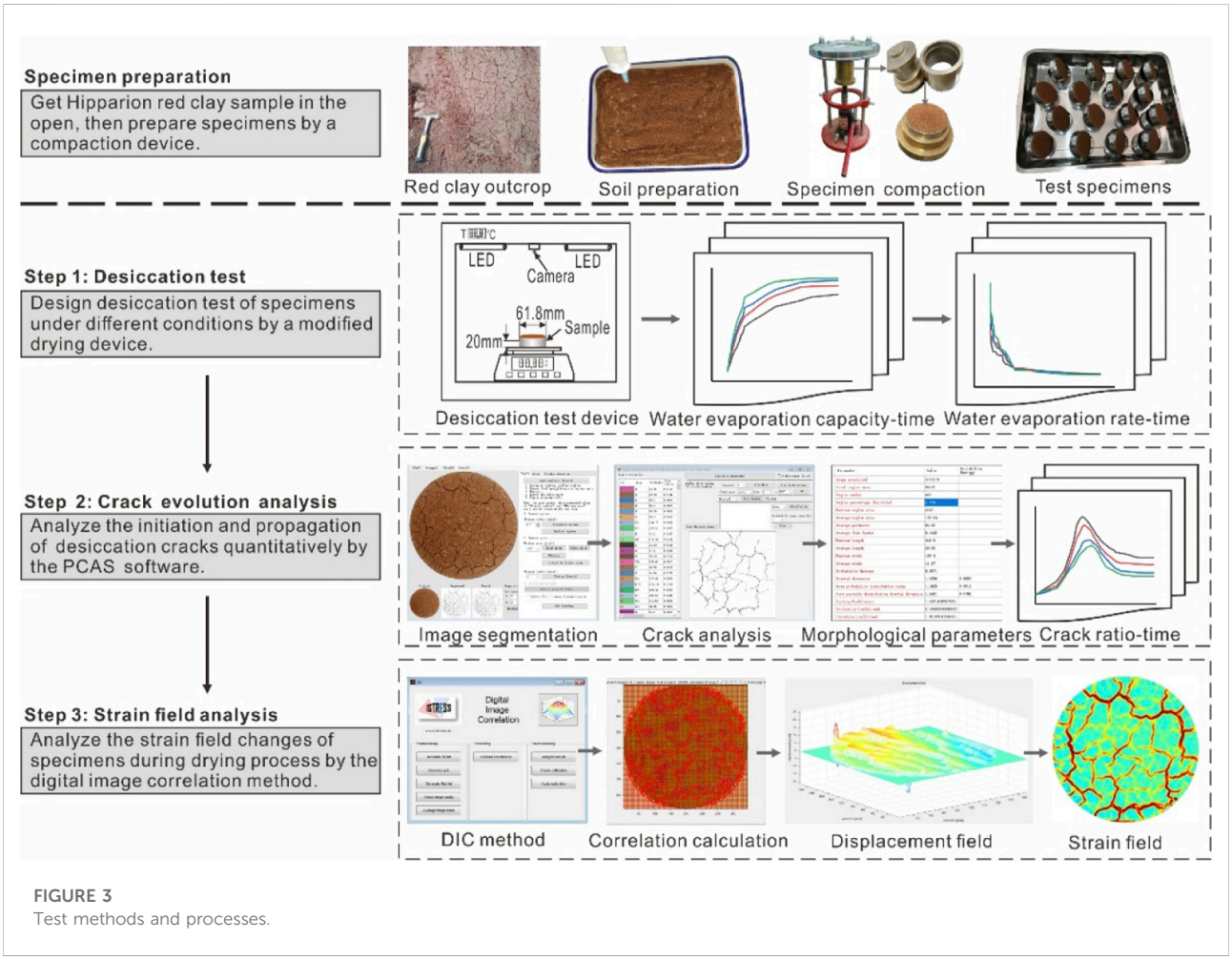

FIGURE 3
Test methods and processes.

TABLE 1 Desiccation test scheme.

Test group	Dry density/g·cm^{-3}	Water content/%	Environmental temperature/°C
1	1.70	12.0,13.5,15.0,16.5,18.0, 19.5,21.0	40
2	1.50,1.55,1.60,1.65, 1.70,1.75,1.80	22.0	40

specimens was carried out using a modified drying device. A thermostat incubator made in China (model SPX-8085H) was modified to allow for installation of a balance and a digital camera (Du et al., 2019). The real-time loss of water content of specimens during drying was monitored by the balance (with an accuracy of 0.01 g). Photos of the desiccation cracks on the specimen surface were automatically taken by the digital camera and then transmitted to a computer terminal. In this modified drying device, the temperature could be set at 40°C to conduct desiccation tests. As drying started, the quality of compacted specimen during drying was continuously monitored by the balance and recorded every 1-min. The camera captured the progressive development of surface cracks in specimen transiting from the initial state to the eventual dried state at 1-min intervals.

For quantitative analysis of the desiccation cracks, PCAS software (Liu et al., 2011, 2013) was used to carry out operations such as image segmentation, spot removal, and crack network identification (Figure 3). Based on top surface digital camera images of specimen during drying, two-dimensional morphological parameters of the desiccation cracks during drying can be obtained. In laboratory measurements, the drying induced volume change of compacted specimens occurs in the form of lateral overall shrinkage (i.e. annular gap develops between the rigid ring and the desiccated clay specimen, and cracks development within the desiccated clay specimens) (Julina and Thyagaraj, 2018, 2019). In previous literature, crack intensity factor (CIF) is defined as the ratio of crack area to the initial total surface area of soil specimen during drying (Miller et al., 1998; Yesiller et al., 2000; Tang et al., 2008, 2010, 2011a, 2011b, 2012; Peron et al., 2009), which captures the total crack area changes (i.e. including annular gap and cracks). In this paper, in order to observe the evolution of desiccation cracks in compacted specimen during drying, we define the surface cracks intensity factor (SCIF) as the ratio of cracks area on soil specimen surface during drying to the initial surface area of soil specimen, and define annular gap intensity factor (AGIF) as the ratio of annular gap area on soil specimen during drying to the initial surface area of soil specimen.

The recorded images of specimen surface were analyzed using digital image correlation techniques (DIC) (Sutton et al., 2009) to observe the principal strain distributions for specimen surface during drying. More about the implementation of DIC analysis can be found in studies of Bornert et al. (2011) and Wang et al. (2017, 2018). In this work, we select the images of specimens during different drying stage to analyze the strain field changing on specimen surface using DIC. Firstly, we take the images from the beginning of desiccation until the cracks are well developed (at the end of desiccation), and then we compare the deformed image with the reference image. Furthermore, we calculate the evolution of displacements and strains in the chosen zines in which cracks developed, and at last we analysis the displacement and strains in the vicinities of identified cracks in detail. The correlation subset is in size of 10× 10 pixel, and its local strain is calculated from the displacements of the neighbors. The convention of continuum mechanics is applied here: tensile strain is positive (red), while compressive strain is negative (blue).

3 Results

3.1 Water evaporation

Figure 4 shows the changes of water evaporation capacity (i.e., the water content loss, %) and the water evaporation rate (i.e., the loss of the water content per unit hour, %/h) of the specimen during drying. It is clear that water evaporation capacity of the specimen increased nonlinearly first, and then reached stabilization gradually. Based on the water evaporation rate, three evaporation stages can be divided into three stages: fast-rate evaporation, falling-rate evaporation and residual evaporation. In the fast-rate evaporation stage, the water content loss increased rapidly due to the large difference in the vapor pressure at the soil surface. In the falling-rate evaporation stage, the water loss gradually slowed caused by the increase of water transport resistance from the evaporation surface. In the residual evaporation stage, the drying process stopped with the water evaporation rate gradually falling to zero, because the relative humidity in soil reached equilibrium with the relative humidity in air.

It should be noted that the water evaporation of specimens with different initial water content and dry density differs significantly, especially in falling-rate evaporation and residual evaporation stage. In particular, the evaporation rate increased with the increasing initial water content of specimen during drying (Figures 4A,B), however, the water evaporation capacity of the specimen decreases with the increasing initial water content. In the early stage of drying, the higher the initial moisture content results in the greater the relative humidity of the soil surface, thus the evaporation rate is larger (Figure 4A). In

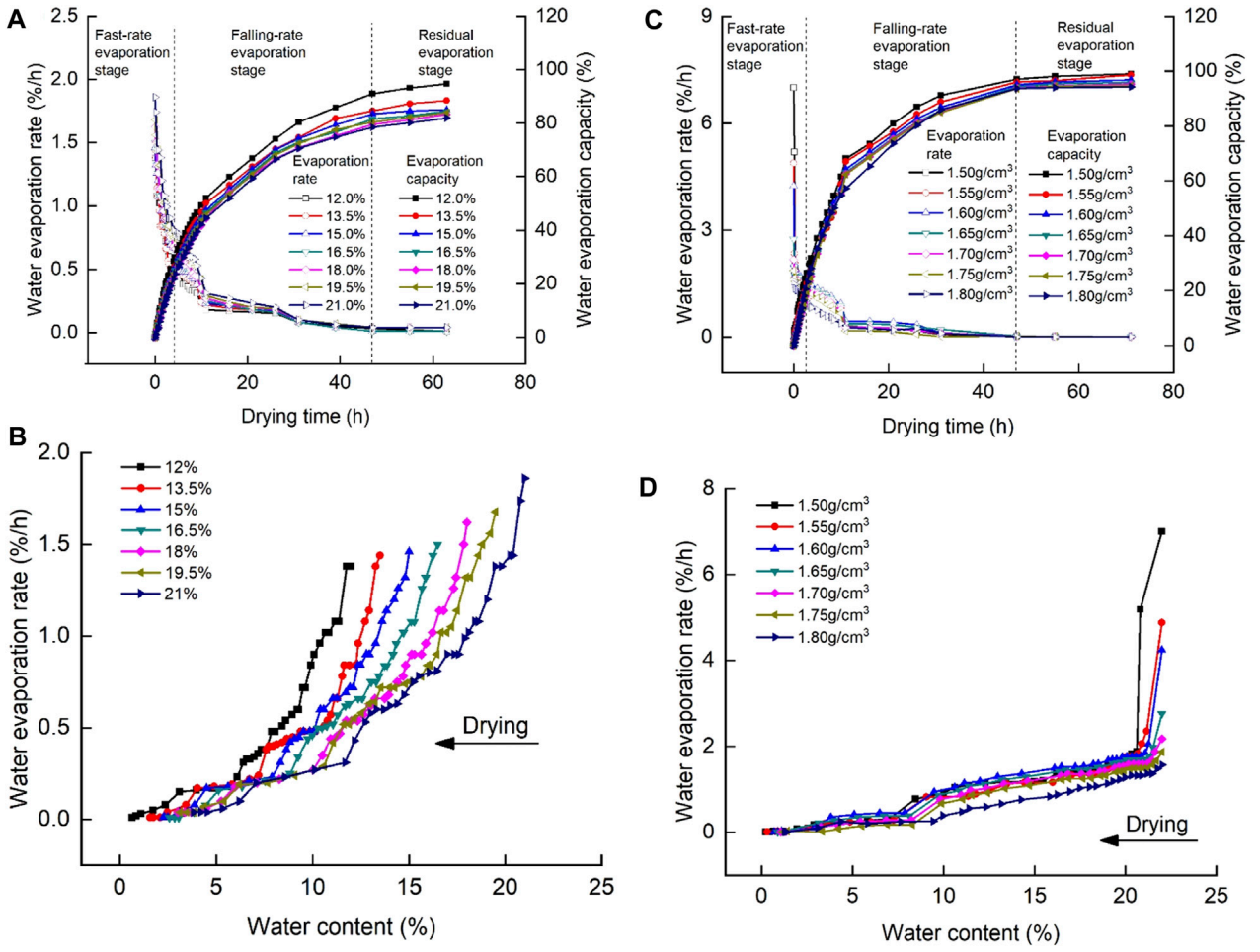

FIGURE 4
Changes of the water evaporation capacity and water evaporation rate of specimens during drying. **(A)** Water evaporation of specimens of different initial water content with time, **(B)** Water evaporation rate of specimens with different initial water content, **(C)** Water evaporation of specimens of different initial density with time, and **(D)** Water evaporation rate of specimens with different initial density.

the late stage of drying, the residual moisture content of specimens increases with the initial water content (Figure 4B). The above evaporation evolution is related to the soil structure differences of compacted specimens with different initial water content (Bai et al., 2021, 2022). The compaction water content has a significant effect on soil structure (Delage et al., 1996). Aggregates and larger inter-aggregate pores in soil samples with low initial water content led to its low water holding capacity as well as low residual water content. On the contrary, soil samples with higher initial water content show well-dispersed structure due to the full hydration of clay particles, and the relatively uniform pores of soil makes its water holding capacity and residual moisture content higher (Nowamooz and Masrouri., 2010b; Burton et al., 2015; An et al., 2018). Therefore, the soil samples with higher initial water content shows lower evaporation capacity, and causes a higher residual water content.

Figure 4C show that the evaporation rate generally decreases with the increasing dry density of specimen, especially in the falling-rate evaporation stage. In addition, the water evaporation capacity decreases with the increasing dry density. Figure 4D shows that the residual moisture content of specimen increase with the increasing dry density in the residual evaporation stage. The above evaporation evolution is related to the soil structure controlled by compaction degrees (Huang et al., 2018). Different compaction degree results in different soil microstructures, which further affects the hydro-mechanical behavior of compacted soils (Mitchell and Soga, 2005; Nowamooz and Masrouri, 2010b). Lower dry density results in larger porosity of soil specimen, which is more conducive to water transmission (Mitchell and Soga, 2005). On the contrary, larger dry density results in the smaller porosity of soil specimen, and the combined water film on the surface of the soil particles overlaps, hindering

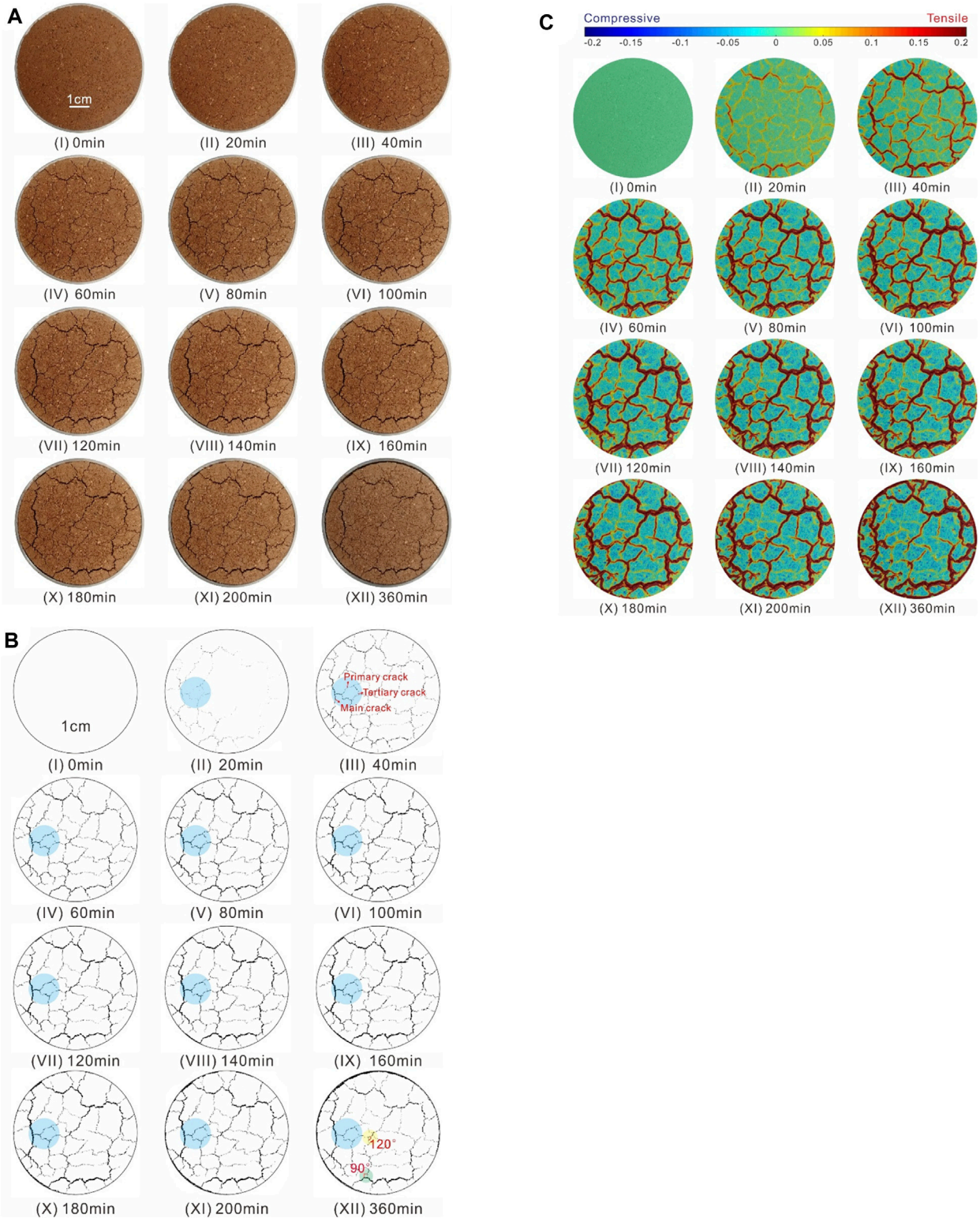

FIGURE 5
Evolution of desiccation cracks for compacted specimen with initial dry density of 1.50 g/cm^3 and initial moisture content of 22%. **(A)** Evolution of crack patterns on the top surface of specimen, **(B)** Evolution of cracks of specimen analyzed by PCAS, and **(C)** Strains field variations of specimen surface during drying.

the flow of capillary water (Romero and Simms, 2008). This is not conducive to water transmission, and thus the evaporation rate is lower. Therefore, the soil specimen with higher dry density shows lower evaporation capacity, and causes a higher residual water content.

3.2 Desiccation cracking and cracks morphology

Typical evolution of desiccation cracks for compacted Hipparion red clay is presented in terms of top surface digital camera images as showed in Figure 5. It is clear that the soil specimen remained intact until the initiation of cracks at 20 min (Figures 5A,BII), followed by the formation of more cracks at 40 min (Figures 5A,BIII). Notably, the lateral shrinkage of specimen include the cracks on specimen surface and the annular gap developed between the rigid ring and specimen. The annular gap did not appear until 60 min, and continuously increased in size during drying (Figures 5A,BIV). The cracks on specimen surface continuously expanded to their peak sizes at 100 min (Figures 5A,BVI), and later the crack self-healing behavior immediately occurred. That is, the crack started to shrink in width and length gradually after spreading to its peak value (Figures 5A,BVI–IX). The development of crack stabilized at about 360 min (Figures 5A,BXII).

The cracks on specimen surface formed a crack network, which can be divided into three types of primary cracks, secondary cracks, and tertiary cracks as shown in Figure 5B. Generally, the primary cracks are those that occur first with the largest length and width, and dominated the evolution of desiccation cracks on specimen surface; the secondary cracks with smaller length and width formed orthogonal to the existing primary cracks, and have scattered distribution; the tertiary cracks with the smallest size occurred between the secondary cracks, and have limited influence on the evolution of desiccation cracks in specimen. Notably, these three type cracks all exhibited self-healing behavior, and the smaller the crack scale was, the more obvious the crack self-healing. In particular, some secondary and tertiary cracks reclosed completely. It should be notes that the self-healing only occurred in cracks, while the annular gap between rigid ring and specimen did not generate self-healing behaviors.

Figure 5B highlight the cracks can't be categorized as pure orthogonal or pure non-orthogonal patterns. The crack segments are relatively orthogonal to each other or intersected to each other with an angel of 120°, and the orthogonal cracks significantly dominate the pattern of desiccation cracks. Furthermore, the intersection angle between different type cracks is close to 90°, and the intersection angles between same type cracks is approximately 120° (Figures 5BXII). Peron et al. (2009), Tang et al. (2011a) and Costa et al. (2013a) also reported the intersection angle of the cracks in soils reconstituted from slurries ranged between 80° and 120°. A careful observation of crack pattern after drying shows that the crack network is mainly composed of three types of polygon: quadrilateral, primary shape and pentagon (Figure 5B). The intersection points of the cracks are likely to form "T" and "Y" shapes, and similar observations have been reported in previous studies (Tang et al., 2011b; Hirose and Matsubara., 2018). The formation mechanism of "T" shapes crack can be explained by the maximum stress release criterion and crack propagation criterion proposed by Morris et al. (1992). That is, since the internal stress perpendicular to the existing crack plane has already been released, the propagating crack will approach the pre-existing crack in the direction perpendicular to the local maximum tensile stress. The formation mechanism of "Y" shapes crack can be explained by adopting the concept of Griffith's fracture energy balance. The "Y" shape crack intersection is the most energy efficient, where the crack length required is the minimum for expending the same amount of energy (Kodikara et al., 2000; Costa et al., 2013a).

3.3 Precursor of desiccation cracking

Based on images of cracks recorded during desiccation tests, the DIC technique yields the continuous full-strain measurement on specimen surface as shown in Figure 5C, which shows the precursor of desiccation cracking. Before drying, there was no change of strain field on specimen surface (Figures 5CI). As drying, the crack lips involve high tensile strain (in yellow and red color), indicating the extension of cracks (Figures 5CII). However, in the adjacent zone of the cracks, the compressive strain area with light blue color represents the compression deformation in the corresponding zone due to the shrinkage of specimen. At the early stage of drying, the compressive strain zone on the specimen surface propagates continuously (Figures 5CIII,VI), indicating that the overall shrinkage of the specimen increased continuously. Notably, the cracks region has suffered from significant increase of high tensile strain (in dark red color), indicating that the cracks continuously expanded due to the further shrinkage of specimen. With further drying, the overall shrinkage of specimen increase continually, resulting in the further expansion of compressive strain zone on specimen surface (Figures 5CV–IX). However, the width of high tensile strain zone decreased gradually, which shows the precursory information for crack self-healing that would occur subsequently. The decreasing of dark red tensile strain zone in width indicates the shrinkage of the primary crack in width, and the disappearance of red or yellow tensile strain zone represents the self-healing of secondary cracks and tertiary cracks (Figures 5CV–IX). The increasing red tensile strain zone with a ring shape outer the specimen represents the expansion of annular gap between the rigid ring and the specimen (Figures 5CX–XII). It shows that the overall shrinkage of the specimen increased

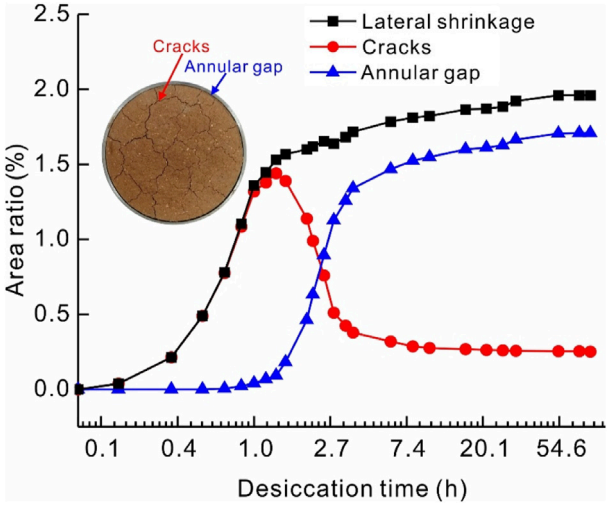

FIGURE 6
Variations of lateral shrinkage of specimen versus drying time. The lateral shrinkage consists of cracks on specimen surface and annular gap between the rigid ring and specimen.

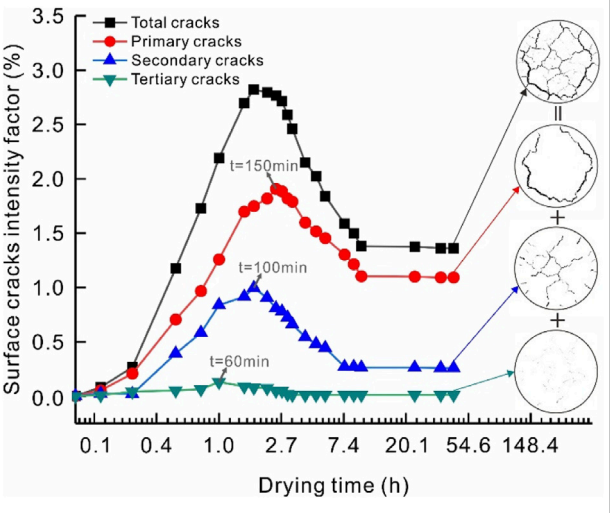

FIGURE 7
Crack ratio Variations of different type cracks versus drying time. The total crack is the sum of primary crack, secondary crack and tertiary crack.

continuously until the end of drying. Gradually, the red tensile strain zone and the blue compressive strain zone on specimen surface gradually stabilized and no longer changed, indicating that the cracking process stopped. In summary, the strain field before onset of cracking already contain precursory information on cracking that would subsequently occur. The increment and reduction of the tensile strain area on specimen surface effectively represents the propagation and self-healing behaviors of desiccation cracks.

3.4 Initiation and propagation of desiccation cracks

Figure 6 shows that the lateral shrinkage of compacted specimen during drying consists of cracks on specimen surface and annular gap between the rigid ring and specimen. To quantify the evolution of cracks and annular gap during drying, we carried out image analysis for all specimens by using the PCAS. Figure 6 shows the variations of surface cracks intensity factor (SCIF) and annular gap intensity factor (AGIF) of specimen during drying. It is obvious that the lateral shrinkage of specimen and the annular gap increase continually until it stabilize to peak values after drying. However, the cracks increase first, and then decreases gradually after its peak value during drying, indicating the appearance of crack self-healing behavior. Notably, the cracks on specimen surface appear first, and then the annular gap representing the global shrinkage of soil specimen appears later. The crack self-healing stage corresponds to the stage for

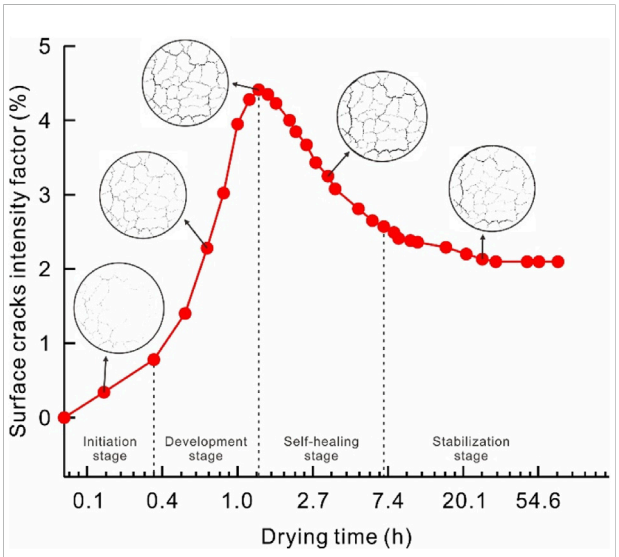

FIGURE 8
Evolution stage of cracks on specimen surface during drying.

the fast increasing of annular gap, which indicates the crack self-healing is caused by the global shrinkage of specimen.

In order to further observe the self-healing of cracks, the variations of crack ratio of primary cracks, secondary cracks, and tertiary cracks are shown in Figure 7. The primary cracks appeared first, and then the secondary cracks and tertiary cracks gradually initiated. The primary cracks and secondary cracks dominated the scale of cracks, and the crack ratio of

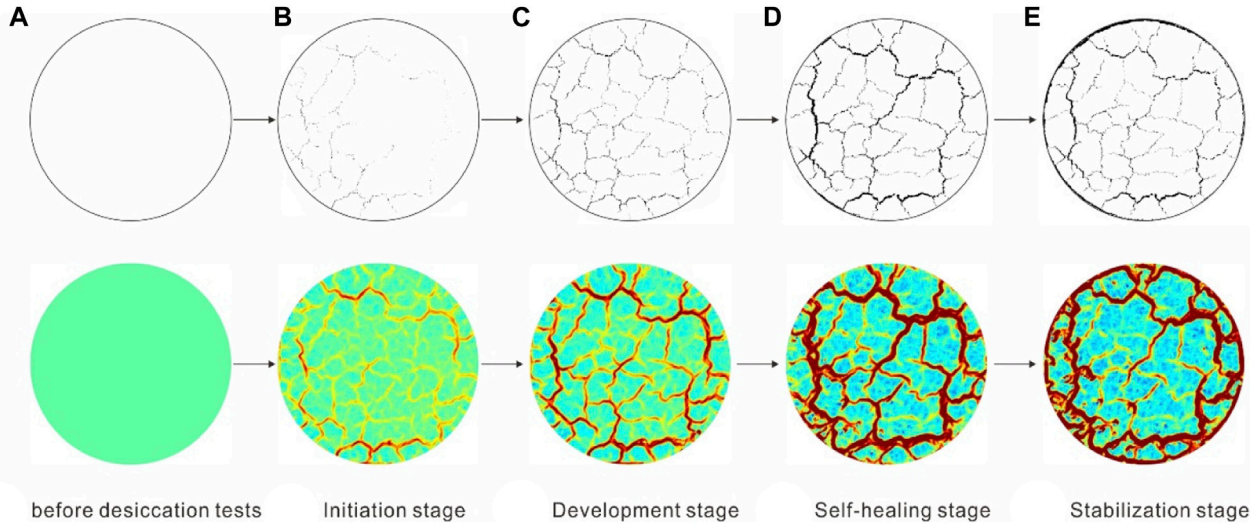

FIGURE 9
Strains field variations of specimen surface during different stages. **(A)** No strains field change before desiccation test, **(B)** Strains field in crack initiation stage, **(C)** Strains field in crack development stage, **(D)** Strains field in crack self-healing stage,and **(E)** Strains field in crack stabilization stage.

tertiary cracks do not vary significantly due to its limited size. Notably, all type cracks exhibited the self-healing behaviors, and the larger the crack scale is, the more obvious the crack self-healing was. Specifically, the primary cracks show the highest crack ratio reduction of 0.82% from peak value of 1.91% to stable value of 1.09%, and the secondary cracks show the reduction in the crack ratio of 0.74% from peak value of 1.00% to stable value of 0.26%. The tertiary cracks present the smallest crack ratio reduction among those three type cracks, with 0.12% reduction from peak value of 0.13% to stable value of 0.01%. Furthermore, the occurrence time of self-healing of each type crack is different. Specifically, the self-healing of tertiary crack occurs the earliest, followed by the secondary crack, and the primary crack. When the secondary cracks generate self-healing shrinkage, the total crack ratio shows a decreasing trend immediately (Figure 7).

Based on the evolution of cracks ratio, the desiccation cracks of compacted Hipparion red clay specimen undergoes four stages including initiation, development, self-healing, and stabilization (Figures 8, 9). In the crack initiation stage (stage I), the cracks initiate with low increment of crack ratio (Figure 8), and the crack network was formed by primary cracks on specimen surface (Figure 9B). In the crack development stage (stage II), the cracks propagate with large increment of crack ratio, and reach the peak value rapidly (Figure 8). In this stage, the secondary cracks and tertiary cracks begin to initiate perpendicular to primary cracks, and subdivide the primary crack network formed by primary cracks into dense secondary crack network (Figure 9B). In the crack self-healing stage (stage III), the crack ratio decreased rapidly and continuously after its peak value (Figure 8), that is, the cracks on specimen surface begin to shrink in size, even some cracks enclosed completely (Figure 9C). In the crack stabilization stage (stages IV), none new cracks appear on the specimen surface even though the evaporation of specimen continues, and the self-healing of cracks gradually stopped (Figure 9D), indicating the end of desiccation cracking process.

3.5 Effect of initial water content and dry density on crack self-healing

Figures 10, 11 shows the evolution of crack ratio of specimens with different initial water content and dry density during drying. Figures 10A,B indicate that the crack ratio of specimen during drying increase with the increasing initial water content of specimen. In particular, the peak crack ratio of specimen increases with the increasing initial water content of specimen obviously (Figure 10A). This is because the water amount and micro pores of specimen increases with increasing initial water content (Delage et al., 1996), hence, the larger water loss and longer drying process led to a larger number of desiccation cracks. Notably, the crack ratio of specimens with different initial water content are time dependent and water content dependent variables. That is, the crack ratio increases first and then decreases with the increasing drying time and with the decreasing of water content during drying. Specifically, the time corresponding to peak crack ratio of specimen increases with the increasing initial water content of specimen (Figure 10A), and water content corresponding to peak crack ratio of specimen during drying also increases with the increasing initial water content of specimen (Figure 10B).

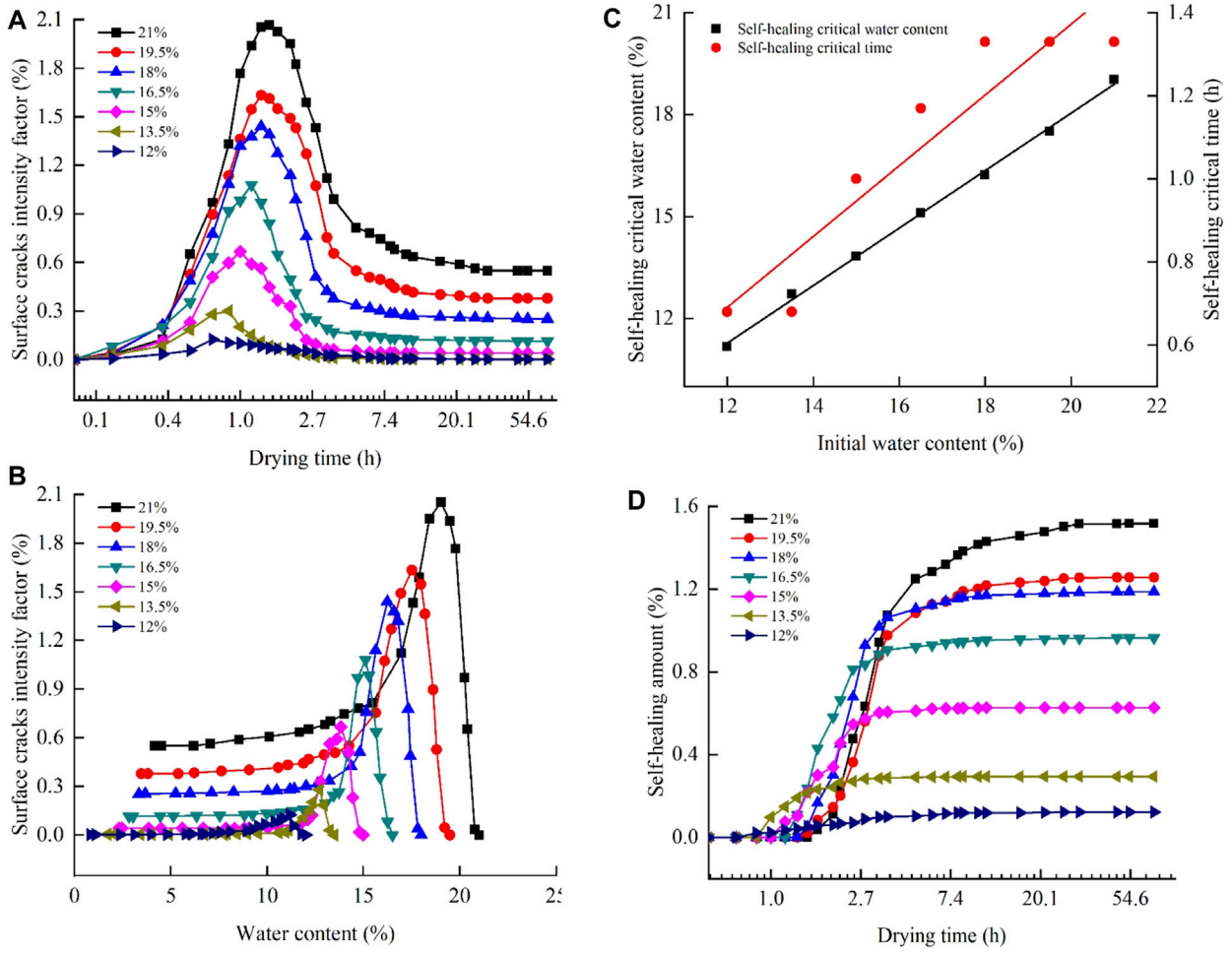

FIGURE 10
Evolution of crack ratio for specimens with different initial water content during drying **(A)** Variation of SCIF with time, **(B)** Variation of SCIF with water content, **(C)** Variation of critical self healing conditions, and **(D)** Variation of self healing amount with time.

As the critical water content is key to study the cracking process of soils (Tang et al., 2021), the cracking water content and shrinkage limit water content, which represent the water content at the onset of cracking and the water content at the stability of cracking, have been paid more attention in previous studies (Tang et al., 2011a.; Tang et al., 2020). While, in this study we observed a new critical water content corresponding to the occurrence of crack self-healing, defined as the crack self-healing critical water content. The cracks ratio of specimen with this water content is maximum, and beyond which it decreased further until the shrinkage limit water content and then stabilized. The cracking water content, the crack self-healing critical water content and the shrinkage limit water content correspond to the special evolution characteristics of crack in the structural, primary shrinkage and residual shrinkage stages respectively during drying (Corte and Higashi., 1964; McGown, 1975; Tang et al., 2011a; Thyagaraj et al., 2017). As the cracking water content and shrinkage limit water content (Corte and Higashi., 1964; Nahlawi and Kodikara., 2006; Rodríguez et al., 2007; Peron et al., 2009; Tang et al., 2011a; Tollenaar et al., 2017), the crack self-healing critical water content of specimen in the primary shrinkage stage is also a non-constant value, which is affected by the initial water content and dry density of specimens (Figure 10C).

Therefore, the critical conditions for crack self-healing and its influencing factors were discussed in this paper. Figure 10C shows that the critical time and critical water content for the occurrence of crack self-healing are affected by the initial water content of compacted specimen significantly. As the initial water content increases, the crack self-healing critical water content increases from 11.17% to 19.03%, and the crack self-healing critical time increases from 0.68 h to 1.33 h. Notably, the self-healing amount of cracks, defined as the reduction value of crack ratio from peak value to the stable value, differs with

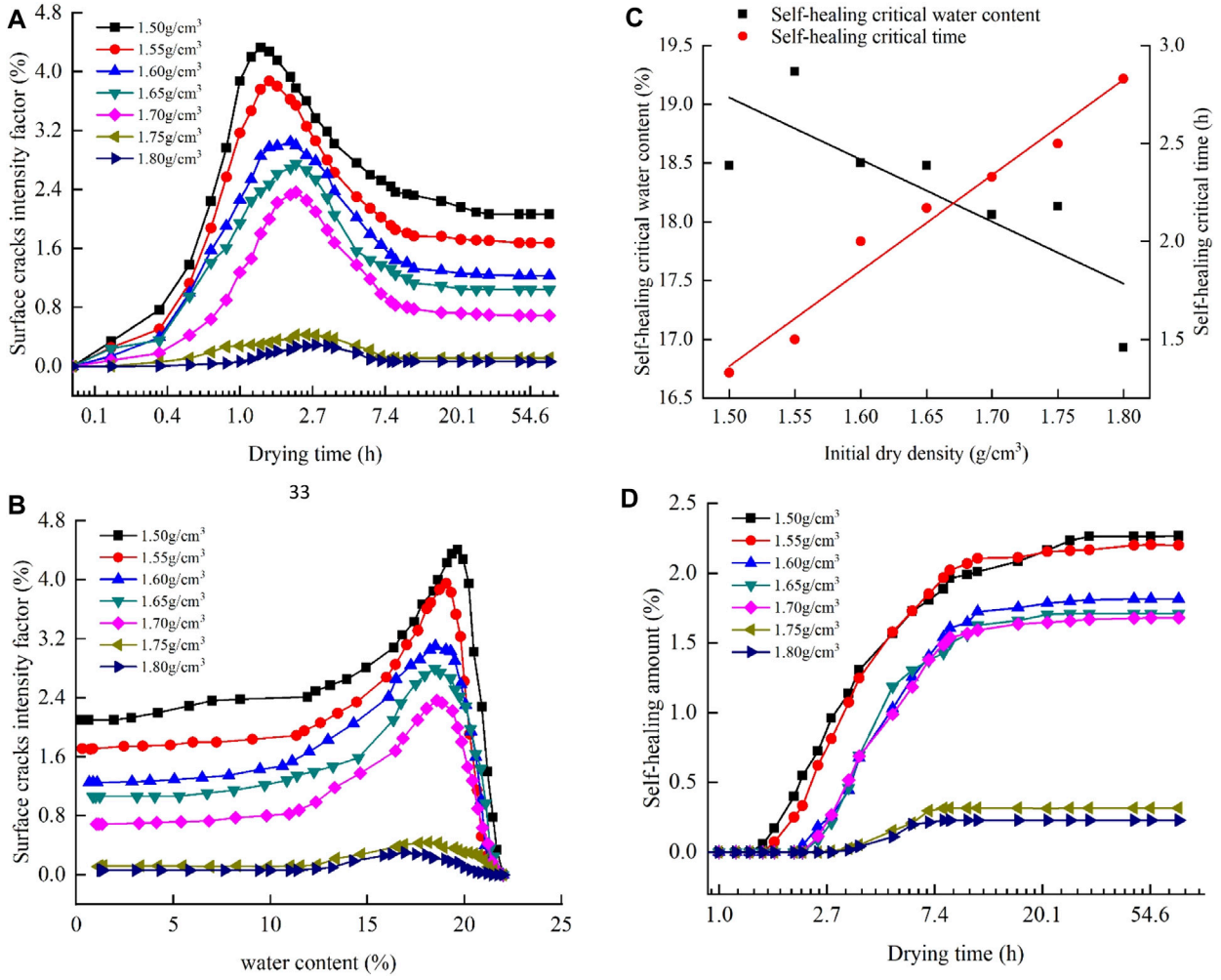

FIGURE 11
Evolution of crack ratio for specimens with different initial dry density during drying **(A)** Variation of SCIF with time, **(B)** Variation of SCIF with water content, **(C)** Variation of critical self healing conditions, and **(D)** Variation of self healing amount with time.

the initial water content of specimens as shown in Figure 10D. Specifically, it is obvious that the self-healing amounts of cracks are initial water content-dependent variables, that is, the self-healing amount increases with the increasing initial water content of compacted specimen. Figure 10 shows the crack ratio of specimens with different initial dry density are also time dependent and water content dependent variables, that is, the crack ratio increases first and then decreases with the increasing drying time and the decreasing water content of specimen (Figures 11A,B). Notably, the maximum crack ratio of specimen increases with the decreasing initial dry density of specimen (Figures 11A,B), that is, the lower the compaction density of specimen, the more cracks the specimen generates. This is because the specimens with lower compactness usually have larger pores and non-uniform distribution of soil particles, hence, water in the specimen evaporates faster during drying process, which results in the propagating of desiccation cracks more quickly and the larger volumetric shrinkage of specimen. While, specimens with the larger volumetric shrinkage contained the larger number of cracks typically (Albrecht and Benson., 2001), thus the crack ratio of specimens increases with the decreasing dry density of specimen. Figure 11C shows that the crack self-healing critical water content and crack self-healing critical time are significantly affected by the initial dry density of specimen. As the dry density of specimen increases, the self-healing critical water content decreases from 18.48% to 16.93%, and the self-healing critical time increases from 1.33 h to 2.83 h. Notably, the self-healing amount of crack differs with the initial dry density of specimen (Figure 11D), that is, the self-healing amount of cracks increases with the decreasing initial dry density of compacted specimen.

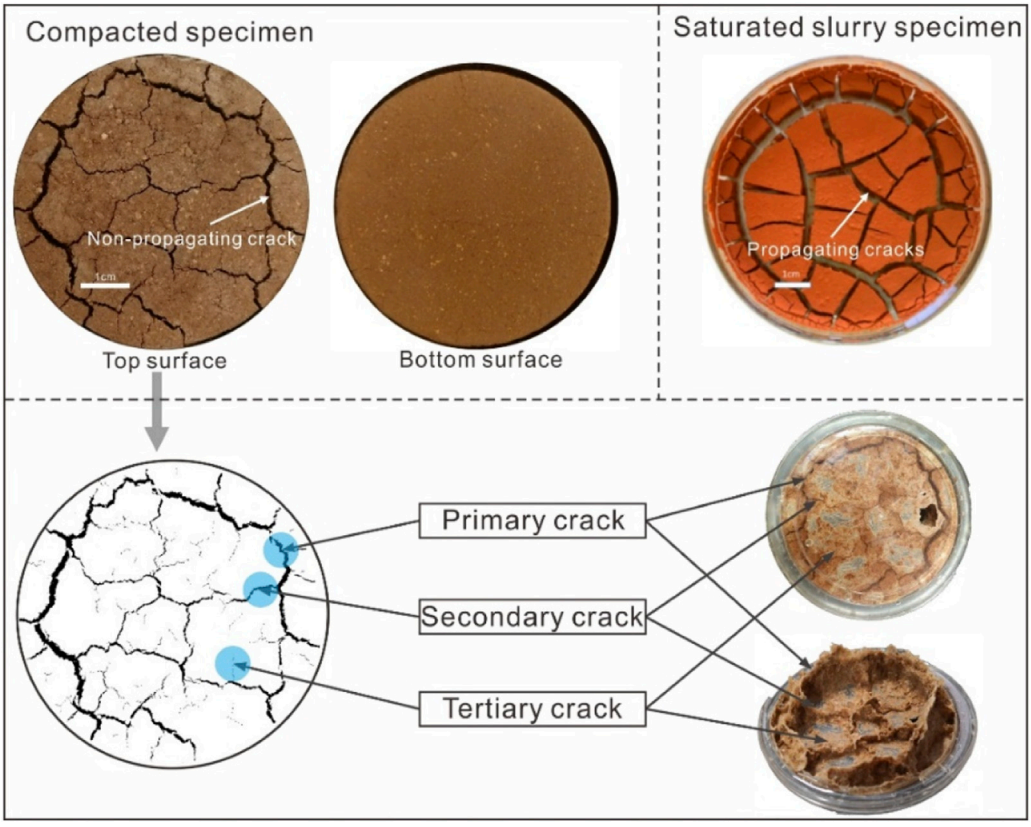

FIGURE 12
Difference of desiccation cracks between saturated slurry and compacted specimen. Propagating cracks in slurry specimen, and non-propagating cracks in compacted specimen.

4 Discussion

4.1 Non-propagating cracking behavior in compacted specimen

Previous studies on cracking of slurry samples indicate that the specimen is separated into many independent soil clods by crack network (Vogel et al., 2005; Peron et al., 2009; Tang et al., 2011a). While, the compacted specimen is not fully separated by soil clods caused by crack network, as the propagation depth of cracks in compacted soils is related to the compactness of specimen (Albrecht and Benson, 2001). Figure 12 shows the different cracks mode between saturated slurry and compacted specimen. Specifically, the desiccation cracks in slurry specimen are mainly propagating cracks extending from top surface to the bottom of specimen. However, the desiccation cracks in the compacted specimen are dominated by the non-propagating cracks (i.e. the cracks do not extend from top surface to bottom of specimen), which have been discussed in our previous study (Du et al., 2019). This difference is caused by the homogeneous structure of slurry samples and heterogeneous structure of compacted samples. Furthermore, the lateral shrinkage in the top part of compacted specimen includes cracks in specimen and annular gap between the rigid ring and specimen, while the lateral shrinkage in the bottom part of the compacted specimen is mainly composed of annular gap. This vertical shrinkage difference in specimen is caused by the differences of water evaporation rate and evaporation capacity between the upper and lower parts of compacted specimen. This originates from the fact that water needs to travel for a longer distance to reach the specimen surface during evaporation when the specimen thickness increases (Kodikara and Choi, 2006).

In order to further verify the non-propagating cracks in compacted specimens, we uses a mixture of epoxy resin and curing agent (phenol sulfonic acid) at a ratio of 3:1 to get the three-dimensional distribution network of cracks in compacted specimen. Firstly, the specimen was completely soaked and the cracks was filled by the gels. In addition, the specimen was placed upside down in a petri dish containing mixed gel for 12 h until the mixed gel got hardened sufficiently. Finally, the specimen was placed in hot water to dissolve specimen soil, and then the crack

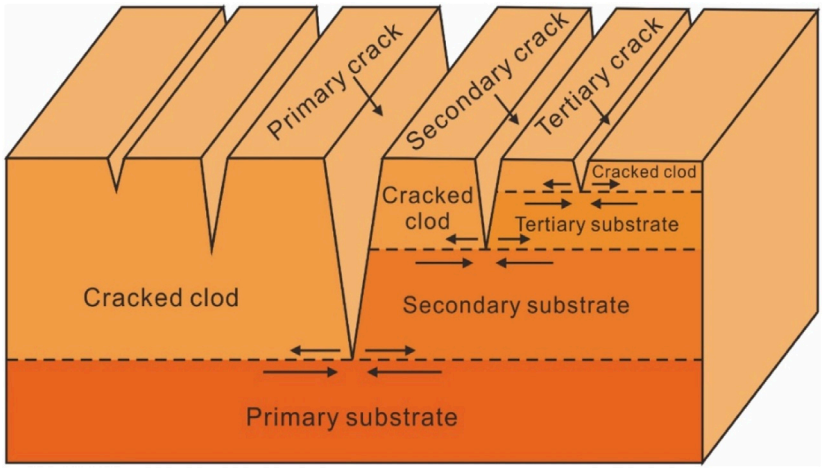

FIGURE 13
Schematic cracking model of specimen during drying. The non-propagating cracks include three types, i.e., the primary crack corresponding to primary substrate, the secondary crack corresponding to secondary substrate, and the tertiary crack corresponding to tertiary substrate.

network composed of hard mixed gel was obtained after the soil was disintegrated completely (Figure 12). The spatial distribution of cracks reveals that the widths and depths of cracks with different types differed greatly, however, none of the cracks penetrated the whole sample in vertical direction. The primary cracks have the largest extension depth, followed by the secondary cracks; the tertiary cracks have the smallest depth.

4.2 Mechanism of crack self-healing

Soil desiccation is a complicated multi-physics process, involving water evaporation, volumetric shrinkage and soil cracking (Bai et al., 2021, 2022). During water evaporation stage, the pore void ratio decreases rapidly with the reduction of water content (Julina and Thyagaraj, 2018), resulting in the volume shrinkage of the sample. The shrinkage deformation results in the initiating and propagating of desiccation cracks on specimens surface (Tang et al., 2021), and the cracking morphology is a good indicator for revealing the shrinkage features of soils (Tang et al., 2011b). Thus, the mechanism of crack self-healing in this paper can be revealed by the vertical anisotropic shrinkage of compacted specimens. In compacted specimen, the water evaporation rate at the top part differed from that at the bottom part (Kodikara and Choi, 2006), which result in the anisotropic shrinkage of specimen in vertical direction.

In order to reveal the vertical anisotropic shrinkage that caused the crack self-healing of specimen, we divided the specimen into two parts along the vertical direction, respectively named as "cracked clods" (soil clods separated by cracks) and "substrate" (specimen soil under the non-propagating cracks) (Figure 13). The substrate can be also classified into three grades corresponding to the different non-propagating crack types, i.e., the primary substrate corresponding to the primary crack, the secondary substrate corresponding to the secondary crack, and the tertiary substrate corresponding to the tertiary crack. The shrinkage of substrate soil drives the crack self-healing, and the different substrate grade with different thickness affected the evolution law of the crack self-healing.

The lateral shrinkage of compacted specimen occurs in the form of annular gap and cracks (Figure 6). The development of annular gap was dominated by the overall shrinkage of substrate soil, and the development of cracks was dominated by the local shrinkage of cracked clods. The occurrence of annular gap represents the overall shrinkage of bottom part of specimen, which corresponds to the peak value of crack ratio on specimen surface (Figure 6). When the amount of crack expansion caused by local shrinkage of cracked clods is smaller than that caused by overall shrinkage of substrate soil, the crack self-healing behavior occurs. In particular, the shrinkage of different grade substrate soil drives its upper different type cracks to shrink with the specimen, resulting in the self-healing of cracks. That is, the self-healing behavior of cracks is attributed to the global shrinkage of substrate soil during drying.

Notably, different initial conditions of compacted specimens, especially the initial water content and dry density, affect the self-healing behavior of desiccation cracks as shown in Figures 10, 11. In order to reveal the influence of the above initial conditions on crack self-healing well, we defined the crack self-healing critical water content as the value for occurrence of crack self-healing, and defined the crack self-healing amount as the reduction value of crack ratio from peak value to the stable value. Specifically, the smaller the initial dry density and the higher the water content of specimen, the larger the self-healing critical water content and the self-healing amount. This is caused by the volume shrinkage difference of specimens with different initial conditions. For

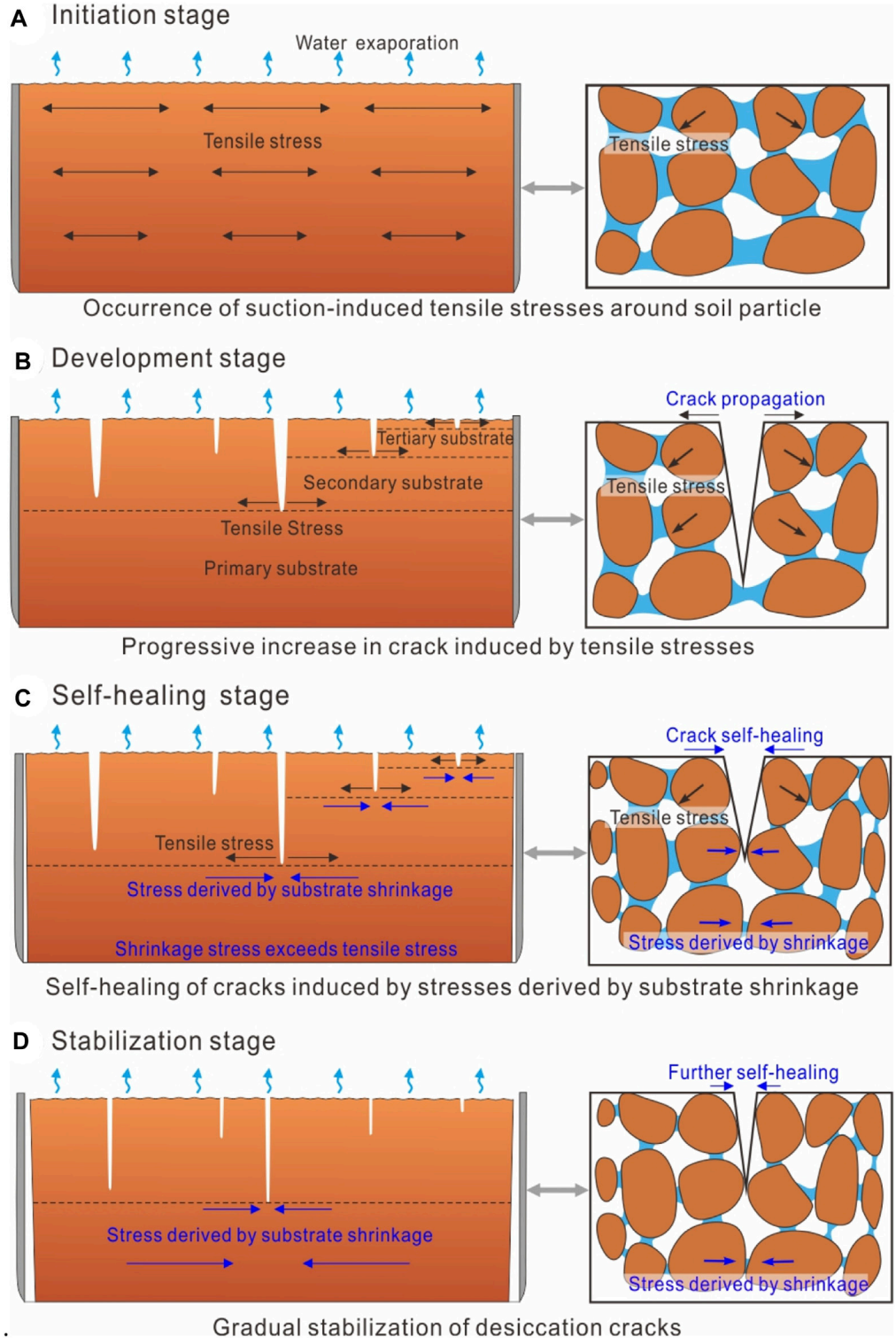

FIGURE 14
Schematic diagram of desiccation cracking mechanism in compacted Hipparion red clay. **(A)** Occurrence of suction-induced tensile stresses around soil particle with water evaporation, **(B)** Crack propagation in different substrate region induced by tensile stresses, **(C)** Occurrence of self-healing of cracks induced by stresses derived by substrate shrinkage, and **(D)** Gradual stabilization of desiccation cracks.

specimen with increasing initial water content, the well-dispersed structure and relatively uniform pores were formed due to the full hydration of particles (Nowamooz and Masrouri., 2010a; Burton et al., 2015; An et al., 2018). The desiccation cracks in compacted specimens with higher water content appears in the void between soil particles, while that in compacted specimens with lower water content appears in the void between aggregates (Cheng et al., 2020). Therefore, the specimens with higher initial water content are prone to generate more desiccation cracks. Additionally, due to the low tensile strength of specimen with higher initial water content, the overall shrinkage of specimen is larger, which results in the larger self-healing critical water content and the self-healing amount. For specimens with increasing initial dry density, the porosity of soil specimen is smaller, and the strength of soil skeleton is higher (Huang et al., 2018). Therefore, the volumetric shrinkage of specimen decreased with increasing compaction dry density. On the contrary, the structure of specimen with smaller initial dry density are composed of aggregates (Tang et al., 2008). The larger pores results in more cracks, and smaller tensile strength of specimens leads to larger volumetric shrinkage. Therefore, the specimens with lower initial dry density generate higher self-healing critical water content and self-healing amount.

4.3 Mechanical mechanism of cracking

The cracking of soils are the result of key processes, such as capillary pressure, suction and tensile stress during evaporation process. In the crack initiation stage (Figure 14A), as the water evaporates during drying, the radii of curvature of the menisci decrease and lead to an increase in the soil suction (Tang et al., 2021). The increase in suction exerts tensile stress at soil particles in the specimen (Figure 14A), and when the suction-induced tensile stress exceeds the tensile strength of soil within the upper layer of the specimen, the desiccation cracks initiate (Tang et al., 2011b; Tabassum and Bheemasetti., 2020). In the crack development stage (Figure 14B), the continuous water evaporation in specimen causes the water membrane to turn thinner continuously, inducing the particle rearrangement and closer packing in specimen. This grain-scale change causes the continuous volume shrinkage of specimen with macro-scope scale. Thus, the cracks continued to propagate downward due to the tensile stress concentration at the crack tips, and the substrate units with different grade and cracks with different type formed in this stage.

In the crack self-healing stage (Figure 14C), as the water continuously traveled to the upper water-air interface during drying, the global shrinkage of the substrate soil below the non-propagating cracks increased continuously. Then the stress derived by substrate soil shrinking have acted on both sides of cracks as shown in Figure 14C, and the value of this stress have been measured by a built-in sensor in the specimen as Sawada et al. (2021), Cheng et al. (2020) and Zeng et al. (2018) reported. The tensile stress acting on soil particles on both side of cracks caused the continuous expansion of crack, and the stress derived by substrate soil shrinking causes continuous shrinkage of cracks in size. The expansion of crack and shrinkage of cracks are opposite in directions, and the magnitude relationship between them determines whether the cracks expand continuously or shrinkage suddenly. As the shrinkage of substrate soil gradually increased, the crack shrinkage value will exceed the crack expansion value, and then the crack self-healing appears (Figure 14C). It should be noted due to the anisotropic evaporation rate in the vertical direction of specimen soil, the shrinkage of tertiary substrate occurs first, driving the self-healing of tertiary cracks first. Then the shrinkage of secondary substrate occurs, driving the self-healing of secondary cracks and tertiary cracks. Finally, the shrinkage of primary substrate occurs, driving the primary cracks, secondary cracks and tertiary cracks to shrinkage in size simultaneously.

During the crack stabilization stage (Figure 14D), as the water content in specimen decreases to the shrinkage limit water content, the evaporation of water gradually stops. Then the shrinkage of the substrate of specimen ceases gradually, causing cracks to stop developing gradually. The specimen shows an inverted cone shape after drying, which reflects the different shrinkage between the upper part and lower part of specimen. In particularly, the lower part of specimen is dominated by the shrinkage form of annular gap, and the upper part of specimen is dominated by the shrinkage form of cracks.

5 Conclusion

The desiccation cracking behaviors of compacted Hipparion red clay specimens with different initial conditions were identified and evaluated using a purpose-made drying device, a crack analysis system and digital image correlation technique. Based on the definition of surface crack ratio, the evolution stages of cracks were divided. Based on the definition of critical water content and self-healing amount, the effect of initial water content and dry density on crack self-healing were discussed. The main conclusions are shown as follows:

(1) The lateral shrinkage in compacted Hipparion red clay specimens during drying consists of non-propagating cracks and propagating annular gap. The annular gap ratio increases with the reducing water content of specimens during drying. While, the cracks ratio increases firstly, and decreases as the global shrinkage of specimen during drying. That is, the crack exhibits self-healing behavior during its evolution, and the width of cracks in the intermediate stages of drying is larger than that observed at the end of drying.

(2) The desiccation cracks in compacted Hipparion red clay specimens undergoes four stages including initiation, development, self-healing and stabilization. The crack self-healing behavior is affected by the initial conditions of compacted specimens. Specifically, the critical water content for

crack self-healing and self-healing amount are not constant values but depend on the initial water content and dry density of specimen. The higher initial water content and lower dry density of specimen will cause larger crack self-healing amount.

(3) The non-propagating cracks in compacted specimen are necessary for crack self-healing behavior. The shrinkage of the substrate soil below the non-propagating cracks drives its upper soil moving towards the center of specimen. As the crack shrinkage value caused by the stress derived by substrate soil shrinking exceeds the crack expansion value caused by tensile stress on soil particles, the crack self-healing behavior of specimen appears.

The study highlights the effect of initial water content and dry density on crack self-healing of compacted Hipparion red clay, and reveals the crack self-healing difference is attributed to the vertical anisotropic shrinkage of specimen due to its pore structure difference. However, this paper represents the cracking behavior of compacted specimen with a fixed size (a height of 20 mm and a diameter of 61.8 mm). More desiccation tests of compacted specimens with different heights are being designed to discuss the critical conditions for crack self-healing, so as to provide a new perspective for revealing the mechanism of the desiccation cracking in clayey soils.

Data availability statement

The original contributions presented in the study are included in the article/Supplementary Material; further inquiries can be directed to the corresponding authors.

Author contributions

YL and BF conducted the test. YZ and HZ wrote the paper. YL and CD made figures. HL and LL provided article revision.

Funding

This study was financially supported by the National Natural Science Foundation of China (41877247, 41790443 and 42041006).

Conflict of interest

The authors declare that the research was conducted in the absence of any commercial or financial relationships that could be construed as a potential conflict of interest.

Publisher's note

All claims expressed in this article are solely those of the authors and do not necessarily represent those of their affiliated organizations, or those of the publisher, the editors and the reviewers. Any product that may be evaluated in this article, or claim that may be made by its manufacturer, is not guaranteed or endorsed by the publisher.

References

Al-Homoud, A. S., Basma, A. A., Husein Malkawi, A. I., and Al Bashabsheh, M. A. (1995). Cyclic swelling behavior of clays. *J. Geotech. Engrg.* 121 (7), 562–565. doi:10.1061/(asce)0733-9410(1995)121:7(562)

Albrecht, B. A., and Benson, C. H. (2001). Effect of desiccation on compacted natural clays. *J. Geotech. Geoenviron. Eng.* 127 (1), 67–75. doi:10.1061/(asce)1090-0241(2001)127:1(67)

An, N., Tang, C. S., Xu, S. K., Gong, X. P., Shi, B., and Inyang, H. I. (2018). Effects of soil characteristics on moisture evaporation. *Eng. Geol.* 239, 126–135. doi:10.1016/j.enggeo.2018.03.028

Auvray, R., Rosin-Paumier, S., Abdallah, A., and Masrouri, F. (2014). Quantification of soft soil cracking during suction cycles by image processing. *Eur. J. Environ. Civ. Eng.* 18 (1), 11–32. doi:10.1080/19648189.2013.840250

Bai, B., Wang, Y ., Rao, D. Y., and Bai, F. (2022). The effective thermal conductivity of unsaturated porous media deduced by pore-scale SPH simulation. *Front. Earth Sci. (Lausanne).* 11 (943853), 1–8. doi:10.3389/feart.2022.943853

Bai, B., Zhou, R., Cai, G. Q., Hu, W., and Yang, G. C. (2021). Coupled thermo-hydro-mechanical mechanism in view of the soil particle rearrangement of granular thermodynamics. *Comput. Geotechnics* 137 (104272), 1–14. doi:10.1016/j.compgeo.2021.104272

Basma, A. A., Al-Homoud, A. S., Malkawi, A. I. H., and Al-Bashabsheh, M. A. (1996). Swelling-shrinkage behavior of natural expansive clays. *Appl. Clay Sci.* 11 (2), 211–227. doi:10.1016/S0169-1317(96)00009-9

Boivin, P. (2007). Anisotropy, cracking, and shrinkage of vertisol samples Experimental study and shrinkage modeling. *Geoderma* 138 (1-2), 25–38. doi:10.1016/j.geoderma.2006.10.009

Bornert, M., Orteu, J. J., and Roux, S. (2011). Corrélation d'images. *Hermes Sci.*, 175–208.

Burton, G. J., Pineda, J. A., Sheng, D. C., and Airey, D. (2015). Microstructural changes of an undisturbed, reconstituted and compacted high plasticity clay subjected to wetting and drying. *Eng. Geol.* 193, 363–373. doi:10.1016/j.enggeo.2015.05.010

Cheng, Q., Tang, C. S., Zeng, H., Zhu, C., An, N., and Shi, B. (2020). Effects of microstructure on desiccation cracking of a compacted soil. *Eng. Geol.* 265, 105418. doi:10.1016/j.enggeo.2019.105418

Chertkov, V. Y., Ravina, I., and Zadoenko, V. (2004). An approach for estimating the shrinkage geometry factor at a moisture content. *Soil Sci. Soc. Am. J.* 68 (6), 1807–1817. doi:10.2136/sssaj2004.1807

Corte, A., and Higashi, A. (1964). *Experimental research on desiccation cracks in soil*, 1–18.

Costa, S., Kodikara, J., and Shannon, B. (2013a). Salient factors controlling desiccation cracking of clay in laboratory experiments. *Geotechnique* 63 (1), 18–29. doi:10.1680/geot.9.P.105

Costa, S., Kodikara, J., and Xue, J. (2013b). *Coupled phenomena in environmental geotechnics: From theoretical and experimental research to practical applications*, 377–381.J-integral as a useful fracture parameter for analysis of desiccation cracking in clayey soils

Day, R. W. (1997). Discussion of "hydraulic conductivity of desiccated geosynthetic clay liners" by tom boardman and david E. Daniel. *J. Geotech. Geoenviron. Eng.* 123 (5), 484–486. doi:10.1061/(asce)1090-0241(1997)123:5(484.2)

Day, R. W. (1998). Discussion: Infiltration tests on fractured compacted clay. *J. Geotech. Geoenviron. Eng.* 124 (11), 1149–1152. doi:10.1061/(asce)1090-0241(1998)124:11(1149)

Day, R. W. (1994). Swell-shrink behavior of compacted clay. *J. Geotech. Engrg.* 120 (3), 618–623. doi:10.1061/(asce)0733-9410(1994)120:3(618)

DeCarlo, K. F., and Shokri, N. (2014). Effects of substrate on cracking patterns and dynamics in desiccating clay layers. *Water Resour. Res.* 50 (4), 3039–3051. doi:10.1002/2013wr014466

Delage, P., Audiguier, M., Cui, Y. J., and Howat, M. D. (1996). Microstructure of a compacted silt. *Can. Geotech. J.* 33 (8), 150–158. doi:10.1139/t96-030

Demagistri, A., Ledesma Villalba, A., Cordero Arias, J. A., Moreno, R., Prat Catalán, P., and Jacinto, A. C. (2018). "Effects of compaction on desiccation cracking of clayey soils," in Unsaturated Soils: UNSAT 2018: The 7th International Conference on Unsaturated Soils (Hong Kong: The Hong Kong University of Science and Technology (HKUST), 1273–1278.

Du, C. C., Zhu, Y. B., Miao, S. S., Gao, M. M., Zhu, J. H., and Zhao, F. S. (2019). The evolution of cracks in the dewatering shrinkage process of hipparion red soil. *Rock Soil Mech.* 40 (8), 3019–3027+3036. doi:10.16285/j.rsm.2018.0885

Goehring, L., Conroy, R., Akhter, A., Clegg, W. J., and Routh, A. F. (2010). Evolution of mud-crack patterns during repeated drying cycles. *Soft Matter* 6 (15), 3562–3567. doi:10.1039/b922206e

Guo, Y., Han, C. J., and Yu, X. (2018). Laboratory characterization and discrete element modeling of shrinkage and cracking in clay layer. *Can. Geotech. J.* 55 (5), 680–688. doi:10.1139/cgj-2016-0674

Hirose, K., and Matsubara, H. (2018). Mechanisms of mudcrack formation and growth in bentonite paste. *J. Geotech. Geoenviron. Eng.* 144 (4). doi:10.1061/(Asce)Gt.1943-5606.0001853

Huang, Z., Wei, B., Zhang, L., Chen, W., and Peng, Z. (2018). Surface crack development rules and shear strength of compacted expansive soil due to dry–wet cycles. *Geotech. Geol. Eng.* 37 (4), 2647–2657. doi:10.1007/s10706-018-00784-y

Julina, M., and Thyagaraj, T. (2018). Determination of volumetric shrinkage of an expansive soil using digital camera images. *Int. J. Geotechnical Eng.* 15 (5), 624–632. doi:10.1080/19386362.2018.1460961

Julina, M., and Thyagaraj, T. (2020). Combined effects of wet-dry cycles and interacting fluid on desiccation cracks and hydraulic conductivity of compacted clay. *Eng. Geol.* 267, 105505. doi:10.1016/j.enggeo.2020.105505

Julina, M., and Thyagaraj, T. (2021). Determination of volumetric shrinkage of an expansive soil using digital camera images. *Int. J. Geotechnical Eng.* 15 (5), 624–632. doi:10.1080/19386362.2018.1460961

Julina, M., and Thyagaraj, T. (2019). Quantification of desiccation cracks using X-ray tomography for tracing shrinkage path of compacted expansive soil. *Acta Geotech.* 14 (1), 35–56. doi:10.1007/s11440-018-0647-4

Kaufhold, S., Dohrmann, R., Klinkenberg, M., and Noell, U. (2015). Electrical conductivity of bentonites. *Appl. Clay Sci.* 114, 375–385. doi:10.1016/j.clay.2015.05.032

Kodikara, J. K., Barbour, S. L., and Fredlund, D. G. 2000. Desiccation cracking of soil layers. *Unsaturated Soils Asia.*:693–698. doi:10.1201/9781003078616-122

Kodikara, J. K., and Choi, X. (2006). A simplified analytical model for desiccation cracking of clay layers in laboratory tests. *Unsaturated Soils* 2006, 2558–2569.

Krisdani, H., Rahardjo, H., and Leong, E.-C. (2008). Effects of different drying rates on shrinkage characteristics of a residual soil and soil mixtures. *Eng. Geol.* 102 (1-2), 31–37. doi:10.1016/j.enggeo.2008.07.003

Lakshmikantha, M. R., Prat, P. C., and Ledesma, A. (2012). Experimental evidence of size effect in soil cracking. *Can. Geotech. J.* 49 (3), 264–284. doi:10.1139/T11-102

Levatti, H. U., Prat, P. C., and Ledesma, A. (2019). Numerical and experimental study of initiation and propagation of desiccation cracks in clayey soils. *Comput. Geotech.* 105, 155–167. doi:10.1016/j.compgeo.2018.09.015

Li, B., Wu, S. R., Shi, J. S., and Feng, Z. (2013). Engineering geological properties and hazard effects of Hipparion laterite in Baoji, Shaanxi Province. *Geol. Bull. China* 32, 1918–1924.

Li, Y. R., Zhang, W. W., He, S. D., and Aydin, A. (2020). Wetting-driven formation of present-day loess structure. *Geoderma* 377, 114564. doi:10.1016/j.geoderma.2020.114564

Liu, C., Shi, B., Zhou, J., and Tang, C. S. (2011). Quantification and characterization of microporosity by image processing, geometric measurement and statistical methods: Application on SEM images of clay materials. *Appl. Clay Sci.* 54 (1), 97–106. doi:10.1016/j.clay.2011.07.022

Liu, C., Tang, C. S., Shi, B., and Suo, W. B. (2013). Automatic quantification of crack patterns by image processing. *Comput. Geosci.* 57, 77–80. doi:10.1016/j.cageo.2013.04.008

McGown, A. (1975). Soil properties and behaviour. *Eng. Geol.* 9 (3), 275. doi:10.1016/0013-7952(75)90009-5

Miller, C. J., Mi, H., and Yesiller, N. (1998). Experimental analysis of desiccation crack propagation in clay liners. *J. Am. Water Resour. Assoc.* 34 (3), 677–686. doi:10.1111/j.1752-1688.1998.tb00964.x

Mitchell, J. K., and Soga, K. (2005). Fundamentals of soil behaviour.

Morris, P. H., Graham, J., and Williams, D. J. (1992). Cracking in drying soils. *Can. Geotech. J.* 29 (2), 263–277. doi:10.1139/t92-030

Nahlawi, H., and Kodikara, J. K. (2006). Laboratory experiments on desiccation cracking of thin soil layers. *Geotech. Geol. Eng.* 24 (6), 1641–1664. doi:10.1007/s10706-005-4894-4

Nowamooz, H., and Masrouri, F. (2008). Hydromechanical behaviour of an expansive bentonite/silt mixture in cyclic suction-controlled drying and wetting tests. *Eng. Geol.* 101 (3-4), 154–164. doi:10.1016/j.enggeo.2008.04.011

Nowamooz, H., and Masrouri, F. (2010b). Influence of suction cycles on the soil fabric of compacted swelling soil. *Comptes Rendus Geosci.* 342 (12), 901–910. doi:10.1016/j.crte.2010.10.003

Nowamooz, H., and Masrouri, F. (2010a). Relationships between soil fabric and suction cycles in compacted swelling soils. *Eng. Geol.* 114 (3-4), 444–455. doi:10.1016/j.enggeo.2010.06.005

Peron, H., Hueckel, T., Laloui, L., and Hu, L. B. (2009). Fundamentals of desiccation cracking of fine-grained soils: Experimental characterisation and mechanisms identification. *Can. Geotech. J.* 46 (10), 1177–1201. doi:10.1139/t09-054

Rao, K. S. S., Rao, S. M., and Gangadhara, S. (2000). Swelling behavior of a desiccated clay. *Geotech. Test. J.* 23 (2), 193. doi:10.1520/gtj11043j

Rodríguez, R., Sánchez, M., Ledesma, A., and Lloret, A. (2007). Experimental and numerical analysis of desiccation of a mining waste. *Can. Geotech. J.* 44 (6), 644–658. doi:10.1139/t07-016

Romero, E., and Simms, P. H. (2008). Microstructure investigation in unsaturated soils: A review with special attention to contribution of mercury intrusion porosimetry and environmental scanning electron microscopy. *Geotech. Geol. Eng.* 26 (6), 705–727. doi:10.1007/s10706-008-9204-5

Sawada, M., Sumi, Y., and Mimura, M. (2021). Measuring desiccation-induced tensile stress during cracking process. *Soils Found.* 61 (4), 915–928. doi:10.1016/j.sandf.2021.03.006

Sutton, M. A., Orteu, J. J., and Schreier, H. (2009). *Image correlation for shape, motion and deformation measurements: Basic concepts,theory and applications*. Incorporated: Springer Publishing Company.

Tabassum, T., and Bheemasetti, T. V. (2020). Self-healing and desiccation crack behavior of kaolinite-rich clay soil. *Geo-Congress* 2020, 582–591.

Tan, L., Zheng, P. L., and Liu, Q. B. (2020). Effects of saline solutions on the desiccation cracking and shrinkage behavior of gaomiaozi bentonite. *Adv. Civ. Eng.*, 1–13. doi:10.1155/2020/8851838

Tang, C. S., Cheng, Q., Leng, T., Shi, B., Zeng, H., and Inyang, H. I. (2020). Effects of wetting-drying cycles and desiccation cracks on mechanical behavior of an unsaturated soil. *Catena* 194, 104721. doi:10.1016/j.catena.2020.104721

Tang, C. S., Cui, Y. J., Shi, B., Tang, A. M., and Liu, C. (2011b). Desiccation and cracking behaviour of clay layer from slurry state under wetting-drying cycles. *Geoderma* 166 (1), 111–118. doi:10.1016/j.geoderma.2011.07.018

Tang, C. S., Cui, Y. J., Tang, A. M., and Shi, B. (2010). Experiment evidence on the temperature dependence of desiccation cracking behavior of clayey soils. *Eng. Geol.* 114 (3-4), 261–266. doi:10.1016/j.enggeo.2010.05.003

Tang, C. S., Shi, B., Cui, Y. J., Liu, C., and Gu, K. (2012). Desiccation cracking behavior of polypropylene fiber-reinforced clayey soil. *Can. Geotech. J.* 49 (9), 1088–1101. doi:10.1139/T2012-067

Tang, C. S., Shi, B., Liu, C., Suo, W. B., and Gao, L. (2011a). Experimental characterization of shrinkage and desiccation cracking in thin clay layer. *Appl. Clay Sci.* 52 (1-2), 69–77. doi:10.1016/j.clay.2011.01.032

Tang, C. S., Shi, B., Liu, C., Wang, B. J., and Gao, W. (2007). Developing law and morphological analysis of shrinkage cracks of clayey soil under different temperatures. *Chin. J. Geotech. Eng.* 29 (5), 743–749.

Tang, C. S., Shi, B., Liu, C., Zhao, L. Z., and Wang, B. J. (2008). Influencing factors of geometrical structure of surface shrinkage cracks in clayey soils. *Eng. Geol.* 101 (3-4), 204–217. doi:10.1016/j.enggeo.2008.05.005

Tang, C. S., Wang, D. Y., Zhu, C., Zhou, Q. Y., Xu, S. K., and Shi, B. (2018). Characterizing drying-induced clayey soil desiccation cracking process using electrical resistivity method. *Appl. Clay Sci.* 152, 101–112. doi:10.1016/j.clay.2017.11.001

Tang, C. S., Zhu, C., Cheng, Q., Zeng, H., Xu, J. J., Tian, B. G., et al. (2021). Desiccation cracking of soils: A review of investigation approaches, underlying mechanisms, and influencing factors. *Earth. Sci. Rev.* 216, 103586. doi:10.1016/j.earscirev.2021.103586

Thyagaraj, T., Thomas, S. R., and Das, A. P. (2017). Physico-chemical effects on shrinkage behavior of compacted expansive clay. *Int. J. Geomech.* 17 (2), 06016013. doi:10.1061/(Asce)Gm.1943-5622.0000698

Thyagaraj, T., and Zodinsanga, S. (2014). Swell–shrink behaviour of lime precipitation treated soil. *Proc. Institution Civ. Eng. - Ground Improv.* 167 (4), 260–273. doi:10.1680/grim.12.00028

Tollenaar, R. N., van Paassen, L. A., and Jommi, C. (2017). Observations on the desiccation and cracking of clay layers. *Eng. Geol.* 230, 23–31. doi:10.1016/j.enggeo.2017.08.022

Tripathy, S., Rao, K. S. S., and Fredlund, D. G. (2002). Water content - void ratio swell-shrink paths of compacted expansive soils. *Can. Geotech. J.* 39 (4), 938–959. doi:10.1139/t02-022

Tripathy, S., and Subba Rao, K. S. (2009). Cyclic swell–shrink behaviour of a compacted expansive soil. *Geotech. Geol. Eng.* 27 (1), 89–103. doi:10.1007/s10706-008-9214-3

Vail, M., Zhu, C., Tang, C. S., Anderson, L., Moroski, M., and Montalbo-Lomboy, M. T. (2019). Desiccation cracking behavior of MICP-treated bentonite. *Geosciences* 9 (9), 385. doi:10.3390/geosciences9090385

Vo, T. D., Pouya, A., Hemmati, S., and Tang, A. M. (2017). Numerical modelling of desiccation cracking of clayey soil using a cohesive fracture method. *Comput. Geotech.* 85, 15–27. doi:10.1016/j.compgeo.2016.12.010

Vogel, H. J., Hoffmann, H., and Roth, K. (2005). Studies of crack dynamics in clay soil. *Geoderma* 125 (3-4), 203–211. doi:10.1016/j.geoderma.2004.07.009

Wang, L. L., Tang, C. S., Shi, B., Cui, Y. J., Zhang, G. Q., and Hilary, I. (2018). Nucleation and propagation mechanisms of soil desiccation cracks. *Eng. Geol.* 238, 27–35. doi:10.1016/j.enggeo.2018.03.004

Wang, L. L., Bornert, M., and Chancole, S. (2017). Microscopic investigation of the deformation mechanisms of argillaceous rock. *Poromechanics Vi Proc. Sixth Biot Conf. Poromechanics*, 1458–1465.

Wei, L., Chai, S. X., Guo, Q. L., Wang, P., and Li, F. (2020). Mechanical properties and stabilizing mechanism of stabilized saline soils with four stabilizers. *Bull. Eng. Geol. Environ.* 79 (10), 5341–5354. doi:10.1007/s10064-020-01885-w

Wei, X., Gao, C. Y., and Liu, K. (2020). A review of cracking behavior and mechanism in clayey soils related to desiccation. *Adv. Civ. Eng.* 2020, 1. doi:10.1155/2020/8880873

Yesiller, N., Miller, C. J., Inci, G., and Yaldo, K. (2000). Desiccation and cracking behavior of three compacted landfill liner soils. *Eng. Geol.* 57 (1-2), 105–121. doi:10.1016/s0013-7952(00)00022-3

Zeng, Z. X., Kong, L. W., Wang, M., and Sayem, H. M. (2018). Assessment of engineering behaviour of an intensely weathered swelling mudstone under full range of seasonal variation and the relationships among measured parameters. *Can. Geotech. J.* 55 (12), 1837–1849. doi:10.1139/cgj-2017-0582

Zhang, T. W., Deng, Y. F., Cui, Y. J., Lan, H. X., Zhang, F. Y., and Zhang, H. Y. (2019). Porewater salinity effect on flocculation and desiccation cracking behaviour of kaolin and bentonite considering working condition. *Eng. Geol.* 251, 11–23. doi:10.1016/j.enggeo.2019.02.007